Time-domain CSEM modeling with a frequency-domain code

Wim A. Mulder, Shell International Exploration and Production B.V.,
Marwan Wirianto and Evert C. Slob, Delft University of Technology*

SUMMARY

We model time-domain electromagnetic measurements of induction currents for marine and land applications with a frequency-domain code. A robust multigrid solver makes frequency-domain modeling followed by a Fourier transform an attractive choice. An interpolation criterion determines the choice of frequencies. The skin depth for each frequency defines the computational grid at each frequency. Examples illustrate the behavior of the method.

INTRODUCTION

Controlled-source electromagnetic measurements of induction currents in the earth can provide resistivity maps for geophysical prospecting. In marine environments, the current source often employs one or a few frequencies. In shallow sea water or on land, the response of air is dominant and time-domain measurements are more appropriate. Because electromagnetic signals in the earth are strongly diffusive, direct interpretation of measured data can be difficult. Inversion of the data for a resistivity model may provide better results. We therefore need an efficient modeling and inversion algorithm.

For time-domain modeling, there are a number of options. The simplest method uses explicit time stepping, but this is rather costly. The Du Fort-Frankel method (1953) is more efficient, but involves an artificial light speed term. Implicit methods can only compete if a fast solver is available (Haber et al., 2002). Drushkin and Knizhnerman (1994; 1999) proposed a technique based on Lanczos reduction and matrix exponentials. Time-domain solutions can also be obtained from a frequency-domain code after a Fourier transform. Newman et al. (1986) present examples for horizontally layered media.

Mulder and Slob (2007) compared the computational complexity of these methods. The complexity measures computational cost in terms of the number of unknowns without the actual constants that define the run-time of a code. On a grid with $O(n^3)$ points, $O(n)$ per coordinate direction, the explicit scheme has an $O(n^5)$ complexity, whereas the others roughly have an $O(n^4)$ complexity. The frequency-domain approach is an exception and has a complexity of $O(n_f n^3)$, where n_f is the number of frequencies. If n_f is of the same order of magnitude as n or smaller, this is an attractive choice. Moreover, the grid at each frequency can be easily adapted to the skin depth (Plessix et al., 2007). Grid adaptation is more difficult with the other methods.

Here we describe the issues arising when using a frequency-domain code for time-domain modeling. These involve the choice of frequencies, the choice of the discretization grid, interpolation to accelerate convergence, and the need for a robust solver. We present a number of examples to illustrate the performance of the method.

METHOD

We summarize the governing equations and their discretization. Then, we describe the automatic selection of frequencies, followed by a discussion on how the skin depth at each frequency determines the computational grid.

The Maxwell equations and Ohm's law for conducting media in the frequency domain can be written as

$$\imath\omega\mu_0\tilde{\sigma}\hat{\mathbf{E}} - \nabla\times\mu_r^{-1}\nabla\times\hat{\mathbf{E}} = -\imath\omega\mu_0\hat{\mathbf{J}}_s. \qquad (1)$$

The vector $\hat{\mathbf{E}}(\omega,\mathbf{x})$ represents the electric field components as a function of angular frequency ω and position $\mathbf{x}$. The current source is $\hat{\mathbf{J}}_s(\omega,\mathbf{x})$. The quantity $\tilde{\sigma}(\mathbf{x}) = \sigma - \imath\omega\varepsilon_0\varepsilon_r$, with $\sigma(\mathbf{x})$ the conductivity, $\varepsilon_r(\mathbf{x})$ the relative permittivity, $\mu_r(\mathbf{x})$ the relative permeability, and ε_0 and μ_0 their absolute values in vacuum. We adopt the Fourier convention

$$\mathbf{E}(t,\mathbf{x}) = \frac{1}{2\pi}\int_{-\infty}^{\infty}\hat{\mathbf{E}}(\omega,\mathbf{x})e^{-\imath\omega t}d\omega$$

and use SI units in the examples.

In the frequency domain, the multigrid method (Mulder, 2006) allows for a reasonably fast solution of the discretized equations when used as a preconditioner for `bicgstab2`, a conjugate-gradient type iterative method (Van der Vorst, 1992; Gutknecht, 1993). On equidistant or mildly stretched grids, the number of `bicgstab2` iterations required to solve the equations at a given frequency is typically around four, independent of the number of unknowns. One `bicgstab2` iteration involves two multigrid preconditioning steps. With stronger stretching, however, the number of iterations increases dramatically. The grid stretching is necessary because of the artificial boundaries that must be included when the computational domain is truncated to finite size. A more powerful method based on semi-coarsening and line-relaxation (Mulder, 2007) is less sensitive to grid stretching but the required computer time per full `bicgstab2` iteration is about 11 times larger. In this multigrid variant, one `bicgstab2` iteration involves six multigrid preconditioning steps, each being more costly than the earlier, simpler multigrid preconditioner. The number of `bicgstab2` iterations is usually about two for problems of practical interest. In spite of its cost, the method becomes attractive with stronger grid stretching. Here, we used the simpler solver if the grid stretching was mild and the more robust solver if the grid stretching was more severe.

The time-domain solutions require a large number of frequencies. We choose an adaptive approach, explained in the description of the first test problem in the next section.

The physics of the problem dictate that at high frequencies, only a small portion of the earth affects the recorded electric field, whereas at lower frequencies, a larger part of the earth is seen. The length scale is controlled by the skin depth $\Delta_s = 503/\sqrt{\sigma f}$, where σ is the conductivity and SI units are used, so Δ_s is in meters. Several conflicting requirements guide the choice of the grid (Plessix et al., 2007):

- Numerical accuracy requires 3 to 8 points per skin depth.
- The grid should be sufficiently fine to honor the details of the resistivity model close to the source and the receivers.
- A point-dipole or finite-length line source generates a singular solution. For receivers at a short distance from the source, the singularity must be resolved with sufficient accuracy, requiring a fine grid. For receivers further away, the solution can have sufficient accuracy without resolving the details of the singularity, thereby requiring a less fine grid around the source.
- As we use perfect electric conductor boundary conditions, a boundary strip of about 5 skin depths is added around the model to avoid undesirable boundary effects. For the air layer, an even thicker layer is added.

The primary-secondary formulation may offer an advantage in some cases. If we abbreviate eq. (1) as $\mathbf{L}\hat{\mathbf{E}} = \hat{\mathbf{f}}$, we can split the linear operator into $\mathbf{L} = \mathbf{L}_p + \mathbf{L}_s$ and the solution into $\hat{\mathbf{E}} = \hat{\mathbf{E}}_p + \hat{\mathbf{E}}_s$ such that $\mathbf{L}_p\hat{\mathbf{E}}_p = f$ and $\mathbf{L}_p$ can be easily solved. The secondary solution is then given by $\mathbf{L}\hat{\mathbf{E}}_s = -\mathbf{L}_s\hat{\mathbf{E}}_p$. If the secondary problem has the same relative magnetic permeability as the primary problem, then $\mathbf{L}_s = \imath\omega\mu_0(\tilde{\sigma} - \tilde{\sigma}_0)$. The secondary problem is as difficult to solve

as the original one, but the advantage is a potentially more accurate solution. If the source resembles a delta function, the solution will be singular close to the source. If a receiver is located close to the source, a rather fine grid is required to resolve the singular behavior of the electric field. If the formation has a conductivity $\tilde{\sigma}_0$ around the source and $\mathbf{L}_s = \imath\omega\mu_0(\tilde{\sigma} - \tilde{\sigma}_0)$ is non-zero sufficiently far away from the source and does not have the character of an isolated point scatterer, the secondary field will generally be less singular. Therefore, a different grid can be used that does not require very small cells close to the secondary source.

RESULTS

Homogeneous formation

The first example is a point current source $\mathbf{J}_s = \mathbf{j}_s\delta(\mathbf{x})\delta(t)$, with $\mathbf{j}_s = (1,0,0)^{\mathsf{T}}\,\mathrm{A\,m}$, in a homogeneous formation with a conductivity of $\sigma = 1\,\mathrm{S/m}$. The frequency-domain solutions were computed on a grid which was adapted to the skin depth and finest near the source. Power-law grid stretching (Mulder, 2006) was applied away from the source. The grid was different for each frequency. The `bicgstab2` iterations were stopped as soon as the norm of the residual dropped below 10^{-6} times the norm of the residual obtained for a zero electric field. Figure 1 shows the real and imaginary parts of E_1, the x-component of the electric field, measured by a single receiver at 900 m distance from the source at the same depth. The computational grid had 128^3 cells. First, solutions were computed at five frequencies $f = 10^q\,\mathrm{Hz}$, with $q = -2,-1,0,1,2$, so $\Delta q = 1$. Zero initial values were used for the electric fields. Next, the computed values of the electric field recorded at the receiver for each frequency f_m were compared to a prediction based on piecewise cubic Hermite interpolation using the values at the other frequencies f_k, excluding the one for which the prediction was made ($k \neq m$). If the relative difference between the interpolated and actual value exceeded 1%, frequencies at $q = q_m \pm \frac{1}{2}\Delta q$ were selected for the next level of computations. From the circles in Figure 1, it can be seen that all four values between $q = -1.5,-0.5,0.5,1.5$ were included. Initial values for the electric fields were now based on cubic Lagrange interpolation using solutions for the four frequencies nearest to the current one. Next, the relative difference between interpolated and computed receiver values was considered again for all available frequencies, and new neighboring values for q at a spacing of $\Delta q = 1/4$ were selected if the relative difference exceeded 1%. Figure 1 shows that new values between -1 and 2 were selected. This procedure was repeated until all relative differences were less than 1%. At $\Delta q = 1/8$, only nine new frequencies were added and at $\Delta q = 1/16$ no new ones were needed. The resulting values for E_1 are shown in Figure 1 as circles, together with the curves obtained by interpolation and the exact solution (Ward and Hohmann, 1987).

The data points were interpolated by piecewise cubic Hermite interpolation (Fritsch and Carlson, 1980) to an equidistant grid of frequencies and transformed to time by a fast Fourier transform. A comparison to the exact time-domain solution, which can also be found in the chapter by Ward and Hohmann (1987), is shown in Figures 2 and 3. The error are largest at early and late times, due to lack of the lowest and highest frequencies. Also, there is a difference between the peak values of about 1% visible in Figure 2.

Two half-spaces

The above shows that we can accurately compute the frequency- and time-domain solutions in the homogeneous case. Next, we consider two half spaces with $\sigma = 3.0\,\mathrm{S/m}$ and $\varepsilon_r = 80$ for $z < 0$, and $\sigma = 0.5\,\mathrm{S/m}$ and $\varepsilon_r = 17$ for $z > 0$. The source is located at $x_s = 0$, $y_s = 0$, and $z_s = -25\,\mathrm{m}$. Figure 4 shows the amplitude of the in-line electric-field component at the interface (at $x = 100\,\mathrm{m}$, $y = 0\,\mathrm{m}$, $z = 0\,\mathrm{m}$) for a frequency of 0.5 Hz. The numerical solution, computed on a grid with 128^3 cells, agrees well with the exact one.

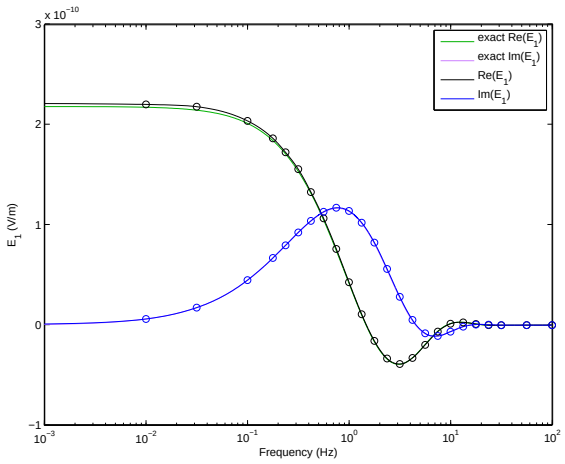

Figure 1: Real(black) and imaginary (blue) part of E_1 for various frequencies. The circles indicate the computed values, the lines were determined by shape-preserving piecewise cubic interpolation. The real and imaginary parts of the exact solution are drawn as well.

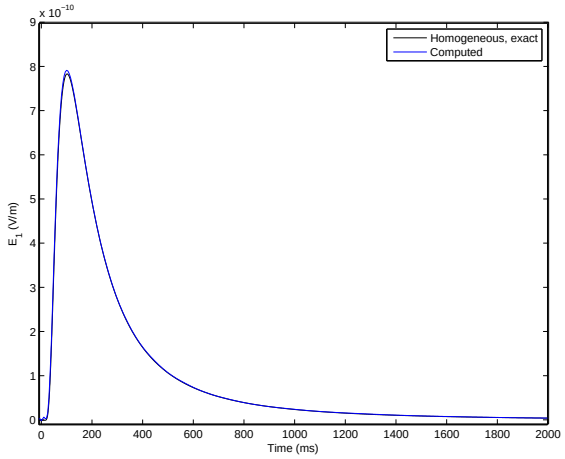

Figure 2: Time-domain solution for the homogeneous problem. Shown in blue is the x-component of the electric field. The exact solution is drawn in black. The peak value has an error of about 1%.

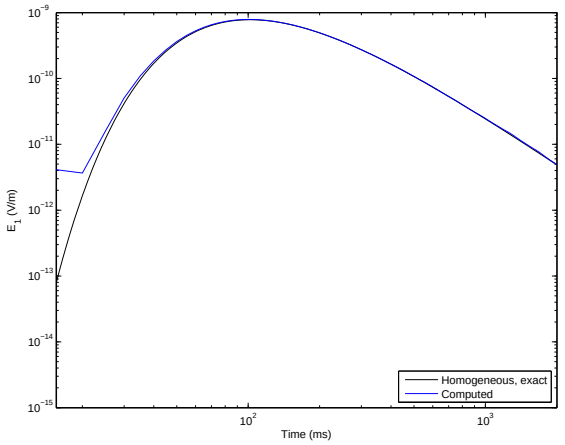

Figure 3: The same time-domain solution for the homogeneous problem as in the previous figure, but now on a logarithmic scale.

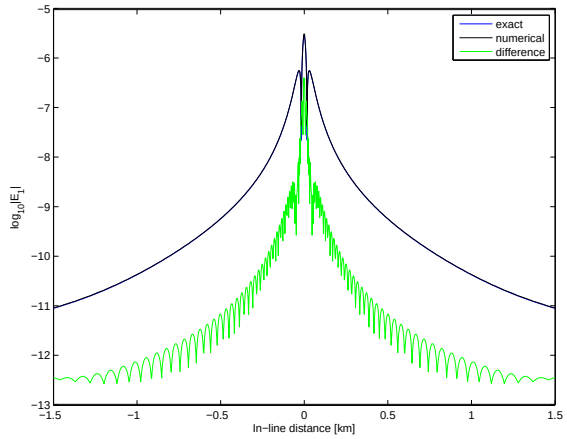

Figure 4: Exact and numerical solution at the interface for the problem with two half-spaces. The logarithm of the absolute value of the error is plotted as well.

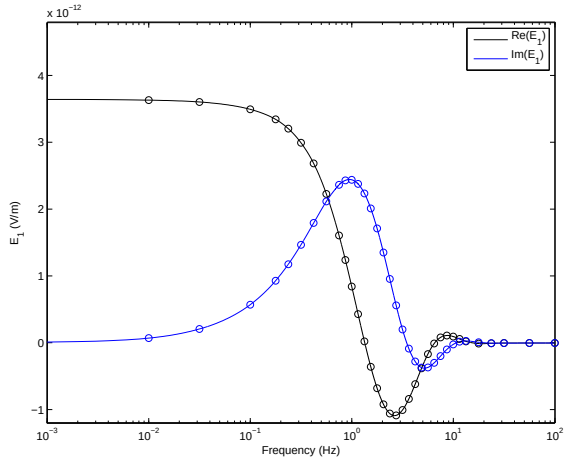

(a)

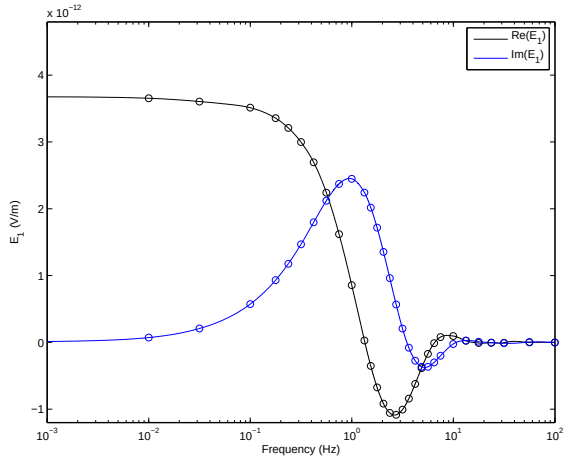

(b)

Figure 5: The top figure shows the secondary solution in the frequency domain computed for grids with 128^3 cells. The bottom one displays the response obtained by taking the difference between the full solutions with and without scatterer.

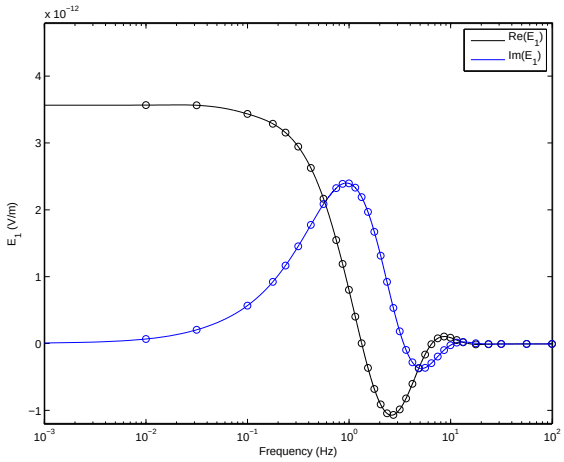

Figure 6: The secondary solution in the frequency domain computed for grids with 64^3 cells.

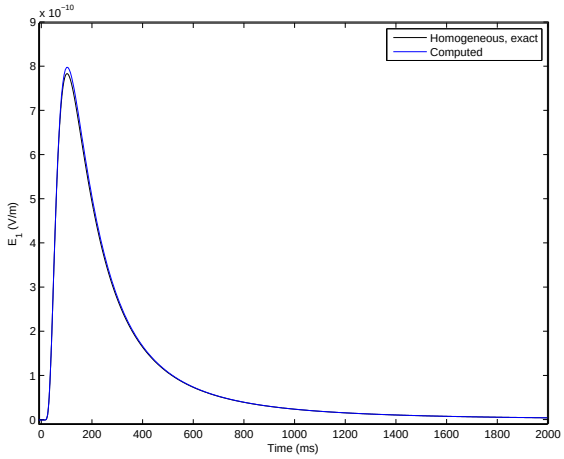

Figure 7: The time-domain solution for the scatterer computed with the primary-secondary formulation on a grid with 128^3 cells. The exact solution for the homogeneous case is shown in black for comparison.

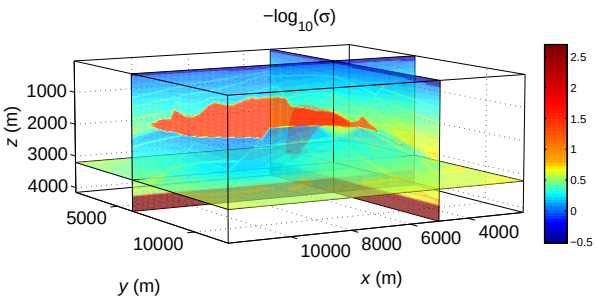

Figure 8: Logarithm of the resistivity ($\log_{10}\sigma^{-1}$, SI units) for a model with a salt body.

Scatterer in a homogeneous formation

The third example is a resistive scatterer in a homogeneous background with a conductivity of 1 S/m. A rectangular scatterer with $x \in (-300,300)$ m, $y \in (-200,200)$ m, and $z \in (400,600)$ m has a conductivity of 0.1 S/m. The source is the same as in the previous example. The grid, however, is different. It is equidistant inside the scatterer and hyperbolic cosine stretching (Mulder, 2006) is applied away from the object. In this case, we used a primary-secondary formulation in which the homogeneous response is subtracted so that the source term and its singular response is replaced by a source term that involves the exact solution.

The frequency-domain solution for a source at the origin and a receiver located at (900,0,0) m and computed on grids with 128^3 cells is displayed in Figure 5(a). For comparison, we have computed the full electric field for the homogeneous medium with the scatterer and subtracted the numerical solution for the homogeneous medium without the scatterer. The difference is shown in Figure 5(b). Since we have subtracted the numerical primary field, its numerical errors in both computations cancel, even when large. This explains the small differences between the figures. Note that the adaptive procedure selected frequencies for the full field that are different from those for the secondary field. The reason is that the primary solution dominates the full field and is different from the secondary solution.

To get an indication of the numerical accuracy, we have repeated the computations for 64^3 cells. The results, shown in Figure 6, should be less accurate. The differences with the computations on 128^3 cells are small. The relative difference is about 3% up till 10 Hz. It increases at higher frequencies as the amplitude tends towards zero.

The time-domain response obtained for the primary-secondary formulation on 128^3 cells is shown in Figure 7. The exact primary solution was added to the computed secondary field and is included for comparison. Because the scatterer has a higher resistivity than its surroundings, the peak in the recorded field is somewhat higher than for the homogeneous case.

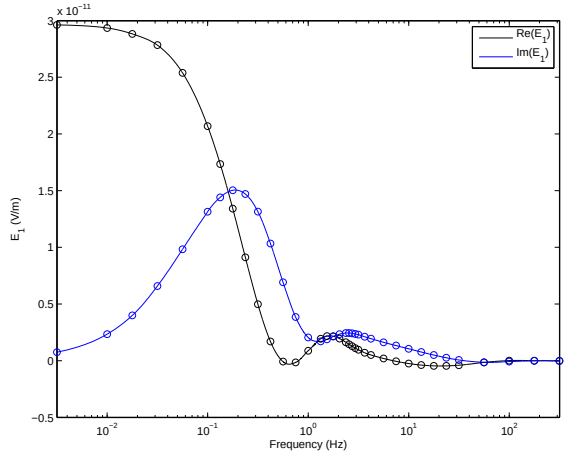

Figure 9: Frequency response for E_1, for a source at (6500,6500,50) m and a receiver at (9000,6500,100) m at the sea bottom.

Shallow marine problem

The SEG/EAGE salt model (Aminzadeh et al., 1997) served as a template for a realistic subsurface model. This model was designed for simulating seismic wave propagation and contains a complex salt body surrounded by sediments. The sea water has depths around 120 m. Its dimensions are 13500 by 13480 by 4680 m. We replaced the seismic velocities of the model by resistivities (σ^{-1}). For the water velocity of 1500 m/s, we chose a resistivity of 0.3 Ohmm. Velocities above 4000 m/s, indicative of salt, were replaced by 30 Ohmm. Basement, beyond 3660 m depth, was set to 0.002 Ohmm. For the resistivity of the sediments, we used $(v/1700)^{3.88}$ Ohmm, with the velocity v in m/s (Meju et al., 2003). For air, we set the resistivity to 10^8 Ohmm. Figure 8 displays the resistivity on a logarithmic scale.

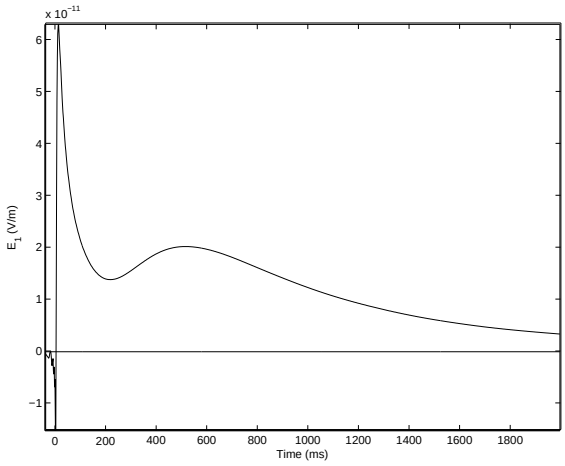

Figure 10: Time response for E_1, for a finite-length source at (6500,6500,50) m and a receiver at (9000,6500,90) m at the sea bottom.

We positioned a finite-length current source between (6400, 6500, 50) and (6600, 6500, 50) m. The receivers were placed on the sea bottom. Initial solutions were computed at frequencies 10^q Hz, with q between -2.5 and 2.5 at a 0.5 increment. More frequencies were added in an adaptive manner. As before, cubic interpolation or extrapolation of solutions for other frequencies provided an initial guess for the iterative solution method. The spatial grid was again based on a balance between the skin depth at the given frequency and the details of the model. In the water layer, the grid was equidistant in the vertical direction and power-law stretching was used away from the surface and maximum depth of the water layer. In the horizontal directions, power-law stretching was applied away from the center of the source. One of the time-domain solutions is shown in Figure 10. The airwave shows up as an early peak. Of course, the air interface will also affect diffusion fronts that come in later. The anti-causal part must be caused by missing high frequencies and numerical errors in the higher frequencies.

CONCLUSIONS

We have synthetized time-domain solutions using a frequency-domain method which has a computational complexity of $O(n_f n^3)$ with n_f the number of frequencies, if the solver convergences in a fixed number of iterations. This could be accomplished on stretched grids by a multigrid variant based on line relaxation and semi-coarsening, whereas on uniform or mildly stretched grids, a simpler multigrid scheme was used. We described the automatic selection of frequencies, the choice of grid depending on skin depth, and the use of monotone piecewise cubic interpolation and a fast Fourier transform to determine the time-domain solutions. After validation against two exact solutions, we applied to code to a realistic marine example.

ACKNOWLEDGMENTS

Marwan Wirianto received financial support from the sponsors of the Delphi consortium.

EDITED REFERENCES

Note: This reference list is a copy-edited version of the reference list submitted by the author. Reference lists for the 2007 SEG Technical Program Expanded Abstracts have been copy edited so that references provided with the online metadata for each paper will achieve a high degree of linking to cited sources that appear on the Web.

REFERENCES

Aminzadeh, F., J. Brac, and T. Kunz, 1997, 3-D salt and overthrust models: SEG.

Druskin, V. L., and L. A. Knizhnerman, 1994, Spectral approach to solving three-dimensional Maxwell's diffusion equations in the time and frequency domains: Radio Science, 29, 937–953.

Druskin, V. L., L. A. Knizhnerman, and P. Lee, 1999, New spectral Lanczos decomposition method for induction modeling in arbitrary 3-D geometry: Geophysics, 64, 701–706.

Du Fort, E. C., and S. P. Frankel, 1953, Stability conditions on the numerical treatment of parabolic differential equations: Mathematics Tables and Other Aids to Computing, 7, 135–152.

Fritsch, F. N., and R. E. Carlson, 1980, Monotone piecewise cubic interpolation: SIAM Journal on Numerical Analysis, 17, 238–246.

Gutknecht, H. H., 1993, Variants of BiCGStab for matrices with complex spectrum: SIAM Journal on Scientific and Statistical Computing, 14, 1020–1033.

Haber, E., U. M. Ascher, and D. W. Oldenburg, 2002, 3D forward modelling of time domain electromagnetic data: 72nd Annual International Meeting, SEG, Expanded Abstracts, 641–644.

Meju, M. A., L. A. Gallardo, and A. L. Mohamed, 2003, Evidence for correlation of electrical resistivity and seismic velocity in heterogeneous near-surface materials: Geophysical Research Letters, 30, 1373–1376.

Mulder, W. A., 2006, A multigrid solver for 3D electromagnetic diffusion: Geophysical Prospecting, 54, 663–649.

———, 2007, A robust solver for CSEM modelling on stretched grids: 69th Conference and Exhibition, EAGE, Extended Abstract, D036.

Mulder, W. A., and E. C. Slob, 2007, TDEM by FDEM: Proceedingsof the Progress In Electromagnetics Research Symposium, 1794–1798.

Newman, G. A., G. W. Hohmann, and W. L. Anderson, 1986, Transient electromagnetic response of a three-dimensional body in a layered earth: Geophysics, 51, 1608–1627.

Plessix, R.-E., M. Darnet, and W. A. Mulder, 2007, An approach for multi-source multi-frequency CSEM modeling in a three-dimensional earth: Geophysics, 72, no. 5.

Van der Vorst, H. A., 1992, BI-CGSTAB: A fast and smoothly converging variant of bi-CG for the solution of nonsymmetric linear systems: SIAM Journal on Scientific and Statistical Computing, 13, 631–644.

Ward, S. A. and G. W. Hohmann, 1987, Electromagnetic theory for geophysical applications, in, M. N. Nabighian, ed., Electromagnetic methods in applied geophysics – Theory, 131–311.